Carbon 146 (2019) 218–223

Contents lists available at ScienceDirect

Carbon

journal homepage: www.elsevier.com/locate/carbon

Cubic Cu_2O on nitrogen-doped carbon shell for electrocatalytic CO_2 reduction to C_2H_4

Hui Ning [a], Xiaoshan Wang [a], Wenhang Wang [a], Qinhu Mao [a], Zhongxue Yang [a], Qingshan Zhao [a], Yan Song [b], Mingbo Wu [a, *]

[a] State Key Laboratory of Heavy Oil Processing, Institute of New Energy, College of Chemical Engineering, China University of Petroleum (East China), Qingdao, 266580, China
[b] CAS Key Laboratory of Carbon Materials, Institute of Coal Chemistry, Chinese Academy of Sciences, Taiyuan, 030001, China

ARTICLE INFO

Article history:
Received 12 December 2018
Received in revised form
27 January 2019
Accepted 4 February 2019
Available online 4 February 2019

ABSTRACT

Electroreduction of carbon dioxide (CO_2) to ethylene (C_2H_4) is one of the most feasible approaches to reduce the carbon emissions and enhance carbon dioxide utilization, whereas the lack of efficient catalysts impedes the scale application. Cuprous oxide (Cu_2O) is a promising catalyst for the formation of C_2H_4 but with unsatisfied selectivity and stability. Herein, we prepared Cu_2O/nitrogen-doped carbon shell (Cu_2O/NCS) composite and employed it in the production of C_2H_4 from CO_2 electroreduction. The ultra-thin NCS with graphene-like structure was prepared from petroleum asphalt by template method. The cubic Cu_2O nanocrystals are uniformly dispersed on the surface of NCS with ca. 150 nm diameters. Cu_2O/NCS loaded on glass carbon electrode showed a high faradaic efficiency of C_2H_4 (24.7%) at −1.3 V (*vs.* reversible hydrogen electrode) as well as remarkable stability. The excellent performance of Cu_2O/NCS is attributed to the high dispersion of cubic Cu_2O nanocrystals and the abundant pyridinic-N moieties in NCS. This work provides a new strategy to improve the selectivity and durability of Cu_2O for production C_2H_4 from electrocatalytic CO_2 reduction by fabricating composites with nitrogen-doped carbon materials.

1. Introduction

Carbon dioxide electroreduction to valued chemicals offers a potential route towards a carbon-neutral society and renewable electricity storage [1–6]. Among all the products of CO_2 electroreduction, ethylene has significant economic value as a massive industrial chemical. However, the development of CO_2 electroreduction to C_2H_4 is hampered by the lack of efficient catalysts. Though huge amount of screened materials has been investigated for CO_2 electroreduction, only copper-based catalysts are known to have a high current efficiency.

Recently, the cuprous oxide (Cu_2O) is investigated as one of the potential catalysts for CO_2 reduction to C_2H_4 [7]. However, the improvement of the selectivity of Cu_2O is hampered duo to the easy aggregation of pristine Cu_2O nanocrystals [8]. In addition, the stability of Cu_2O is not satisfied because of the reduction of Cu^+ to Cu^0 during the CO_2 electroreduction [9]. Thus, it is critical to find an efficient strategy to enhance the selectivity and stability of Cu_2O for massive production of C_2H_4 by CO_2 electroreduction.

Building composites with other materials by supporting strategy is an effective way to improve the electrochemical performance of metal oxides [10–12]. Carbon material has many unique physicochemical properties, such as large surface area, diverse structures, and regulatable functional groups, which makes it a favored candidate to build composites with metal materials for electrochemical applications [13,14]. To be specific, nitrogen doped carbon materials have been found to behave unique activity as catalysts for CO_2 electroreduction, mainly due to the Lewis basicity of pyridinic-N moieties [15–17]. Sun et al. [18] prepared 7 nm Cu nanoparticles assembled on the pyridinic-N rich graphene as catalysis for electrochemical reduction of CO_2. The C_2H_4 formation Faradaic efficiency (FE) reaches 19% at −0.9 V (*vs.* RHE) in 0.5 M $KHCO_3$, which is much higher than pristine Cu. In addition, Mistry et al. [19] reported the stability of Cu^+ under the negative potential can be improved due to the local pH arising, which is derived from hydrogen evolution reaction associating with ion transfer inhibition originated from the confinement effect of rough nanostructures. These works

* Corresponding author.
E-mail address: wumb@upc.edu.cn (M. Wu).

https://doi.org/10.1016/j.carbon.2019.02.010
0008-6223/

predict the selectivity and stability of Cu_2O is very likely to be improved by supporting on a proper nitrogen-doped carbon material for selectivity electroreduction of CO_2 to C_2H_4.

As a low value-added refining product, petroleum asphalt is considered to be a promising feed stock to prepare carbon material due to its relatively high aromatic ring content and carbon yield. However, petroleum asphalt-based carbon material has not been reported as support of Cu_2O for carbon dioxide reduction. Previously, we prepared a carbon shell (CS) material with petroleum asphalt by template method [20,21]. We found the three-dimensional structure of CS is an excellent support to redistribute and stabilize the metal oxides in various electrochemical applications [22].

Herein, we prepared a nitrogen doped carbon shell (NCS) with petroleum asphalt as carbon source and urea as nitrogen source. The cubic Cu_2O nanocrystals were then synthesized and in-situ supported on NCS to obtain Cu_2O/NCS composite. The catalytic performance of Cu_2O/NCS on CO_2 electroreduction was thoroughly investigated and the interaction between Cu_2O nanoparticles and NCS was discussed.

2. Experiment

2.1. Materials and reagents

Petroleum asphalt is obtained from China National Offshore Oil Corporation (17.63 wt% saturates, 31.13 wt% aromatics, 38.21 wt% resins and 6.40 wt% asphaltenes), in which the nitrogen content is 0.78 wt%. Zinc oxide (90 nm) is purchased from Macklin Biochemical Co., Ltd. Hydrochloric acid (36–38 wt%), urea (purity, 99%), Copper chloride dehydrate (purity ≥ 99.0%) are purchased from Sinopharm Chemical Reagent Co., Ltd. Nafion solution (5 wt%) is purchased from Aladdin Industrial Corporation. Sodium hydroxide and ascorbic acid are A.R. grade and purchased from Xilong Scientific. All the chemicals are used as received without further purification. The deionized water (15 MΩ) is produced by a Millipore system in our lab.

2.2. Preparation of CS and NCS

The carbon shell (CS) was prepared according to our previous report [23]. Typically, 4 g petroleum asphalt was dissolved in 70 mL toluene under sonication (700 W) for 30 min. Then 10 g commercial ZnO nanoparticles (90 nm) was added to the solution under stirring. The above mixture was stirred sufficiently at 383 K for 8 h to evaporate toluene completely. The collected solid was transferred to a quartz boat and heated to 1073 K for 2 h in N_2 atmosphere. The obtained product was washed thoroughly with 6 mol dm^3 hydrochloric acid and deionized water until neutral, then vacuum-dried at 333 K overnight to obtain CS. For the NCS preparation, 1.5 g urea was dissolved into 3 mL deionized water, following by adding 0.3 g CS. After ultrasonic dispersing for 0.5 h and vacuum drying for 3 h at 353 K, the obtained powder was subsequently calcined at 800 °C for 2 h under N_2 atmosphere to achieve the NCS.

2.3. Preparation of Cu_2O/CS and Cu_2O/NCS

4 mg CS was dissolved into 3 mL deionized water under sonication for 30 min to obtain a suspension. Then 1.2 mL 0.05 moL/L copper chloride aqueous solution was added into the above suspension under magnetic stirring. After that, 5 mL 0.023 moL/L ascorbic acid water solution was drop wisely added, thus a dark green solution was formed. After vigorously stirring for 2 h at room temperature, the precipitate was filtrated following by washed with ethanol and deionized water thoroughly. After further dried at 333 K overnight, the Cu_2O/CS was obtained. The Cu_2O/NCS was synthesized with the same procedure except that the CS was preplaced by NCS, as illustrated in Fig. 1. As a controlled experiment, the pristine Cu_2O was synthesized following the same procedure except that no CS or NCS was involved.

2.4. Characterization

The crystal property and phase composition of all the materials as-prepared are investigated by X-ray diffraction (X'Pert PRO MPD, Holland) with Cu Ka radiation ($\lambda = 0.15406$ nm). Transmission electron microscopy (TEM, JEM2100UHR, Japan) and field emission scanning electron microscopy (FE-SEM, Hitachi S-4800, Japan) are used to identify the micro-structures and morphologies of the samples. The crystallinity of CS and NCS is labeled by Raman analysis carried out on a LabRAM HR Ecolution Raman spectrometer (Renishaw RM2000, Britain) with 514 nm laser. The elemental composition and valence in the materials as-made are analyzed by X-ray photoelectron spectroscopy (XPS, Escalab 250Xi, UK).

2.5. Electrochemical reduction of CO_2

The electrochemical reduction of CO_2 reactions was carried out at room temperature and atmospheric pressure in a H-type electrolytic cell connected with an electrochemical workstation (CHI 760E, CH Instrument, China). A cation exchange membrane (Nafion® N117, DuPont) divided the H-type electrolytic cell into working and counter electrode chambers, both of which contained 30 mL of 0.1 M $KHCO_3$ as electrolyte. A piece of platinum sheet (1×1 cm^2) was used as the counter electrode and a KCl-saturated Ag/AgCl electrode was used as the reference electrode. To fabricate working electrode, 1 mg sample and 5 μL Nafion solution were dispersed in 200 μL of ethanol. The obtained catalyst ink was ultrasonic treated for 30 min till a homogeneous dispersion was achieved. A glassy carbon electrode (1.2 cm in diameter) was coated with the homogeneous dispersed 1 mg of catalyst using a micropipette.

To start the experiment, the reaction system was purged with high purity Ar (≥99.999%) for 10 min to remove air. The 0.1M $KHCO_3$ solution was saturated with high purity CO_2 (≥99.999%) for 30 min until saturated (pH = 6.8). In the cathodic compartment, the high purity CO_2 gas flow was controlled at 20 mL/min and the solution was stirred at 600 rpm. All the operating voltage was calibrated to the reversible hydrogen electrode (RHE) reference using formula U (versus RHE) = U (versus Ag/AgCl) + 0.197 + 0.0591 × pH [24].

2.6. Analysis of products

The gas-phase products generated during CO_2 electrolysis at each fixed potential were quantitatively analyzed by gas chromatograph (BFRL-3420A, China) which was online connected with the head space of the cathodic compartment. The gas products were injected to the GC using a ten-port valve system with high purity Ar (≥99.999%) as carrier gas. The GC system was equipped with two columns corresponding to the two detectors. The thermal conductivity detector (TCD) was installed to detect hydrogen and carbon monoxide while the flame ionization detector (FID) was fabricated to detect the hydrocarbon products. The liquid-phase products were analyzed using a Shimadzu HPLC LC-20AT system equipped with both refractive index (RID-10A) and UV (SPD-20A) detectors. A Shodex SUGAR SH 1011 column at 60 °C with 0.005 M H_2SO_4 solution as the mobile phase was used to separate and identify the compounds. The Faradaic efficiencies of all the products were calculated as reported [25].

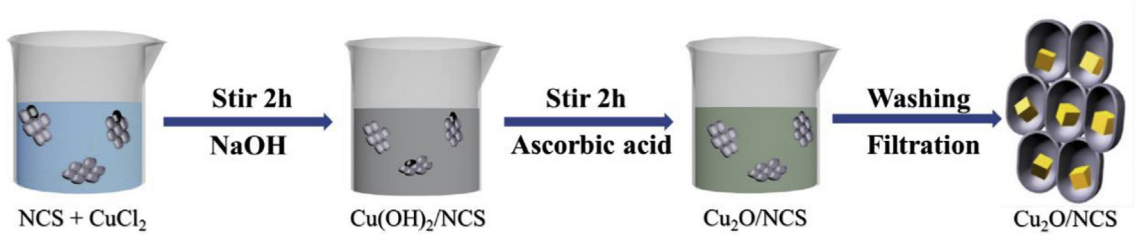

Fig. 1. Synthesis process of Cu_2O/NCS.

3. Results and discussion

As depicted in the SEM images, the CS (Fig. S1a) is an interconnected three-dimensional carbon framework with an open porous texture, which is consistent with our previous works [23]. The NCS (Fig. S1b) has similar morphology with CS, indicating the carbon shell framework is maintained after nitrogen doping.

The pristine Cu_2O (Fig. 2a) prepared without carbon materials are cubic nanocrystals. Interestingly, when the Cu_2O was in-situ supported on the surface of CS, the morphology of Cu_2O nanocrystals changed from cubic to be near-spherical (Fig. 2b) and aggregated obviously. While the CS was replaced by NCS, the Cu_2O nanocrystals maintained cubic morphology and be dispersed uniformly (Fig. 2c). Despite the disparity of morphology, the size of Cu_2O nanocrystals almost behave the similar distribution (ca. 150 nm) in the SEM images of Cu_2O, Cu_2O/CS and Cu_2O/NCS.

Fig. 2d shows the XRD patterns of Cu_2O, Cu_2O/CS and Cu_2O/NCS. Diffraction peaks around 25°and 43° are corresponded to the (002) and (001) planes of CS and NCS [26]. The weak and broadened peaks of CS and NCS indicate the carbon materials as-made are mainly composed of amorphous carbon with low crystallinity. For Cu_2O/CS and Cu_2O/NCS, peaks at 29°, 36°, 42°, 52°, 61° and 73° are accurately indexed to the (110), (111), (200), (211), (220) and (311) planes of Cu_2O nanocrystals (JCPDS NP.05–667) respectively,

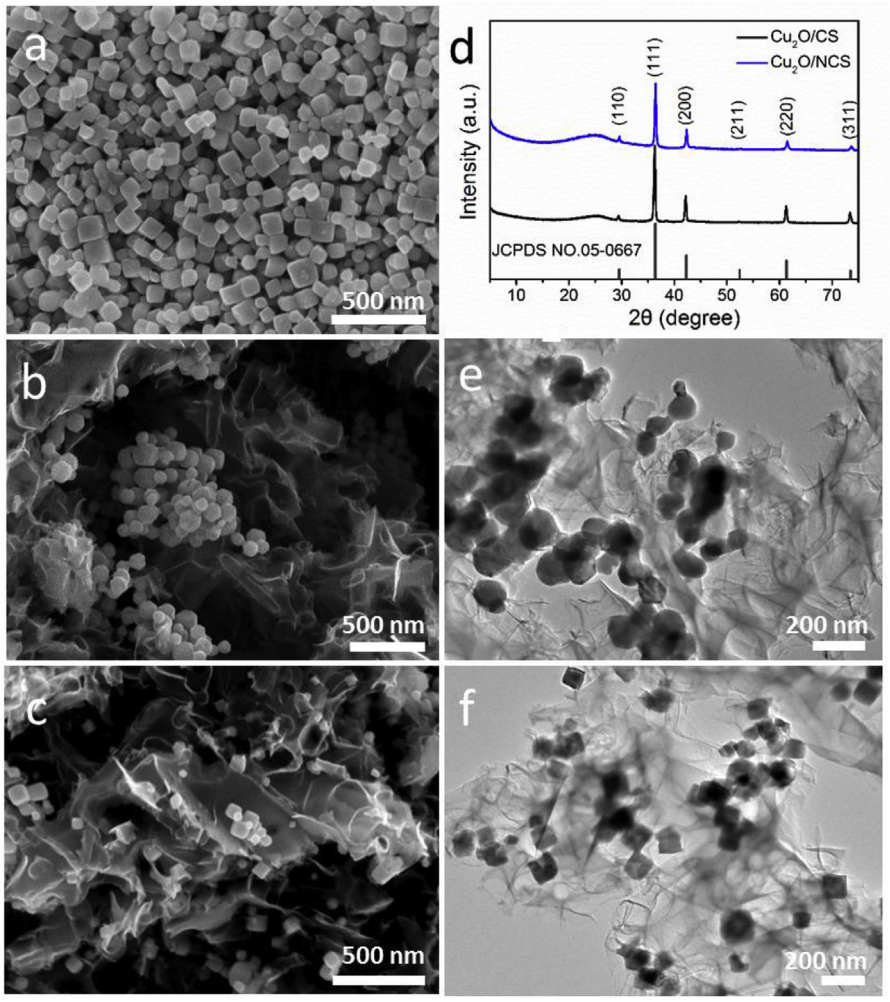

Fig. 2. SEM images of (a) Cu_2O, (b) Cu_2O/CS and (c) Cu_2O/NCS. (d) XRD patterns of Cu_2O/CS and Cu_2O/NCS. TEM images of (e) Cu_2O/CS and (f) Cu_2O/NCS. (A colour version of this figure can be viewed online.)

indicating the Cu_2O nanocrystals are successful prepared and embedded into the surface of carbon materials.

Raman spectra (Fig. S2) represents two typical peaks around 1350 cm^{-1} and 1590 cm^{-1}, corresponding to the disordered sp^3C (D band) and in-plane vibrational sp^2C (G band) [27]. The NCS owns higher intensity ratio of D to G band ($I_D/I_G = 1.23$) compared with CS ($I_D/I_G = 1.15$), indicating NCS has more population of disordered carbon in the graphitic structures due to the nitrogen doping [28]. As depicted in Fig. 3b, high-resolution N 1s spectra of the Cu_2O/NCS is deconvoluted to several Gaussian peaks corresponding to three types of N-binding modes, pyridinic-N (398.5 eV), pyrrolic-N (400.8 eV) and quaternary-N (402.2 eV), which is consistent with CS, NCS and Cu_2O/CS (Fig. S4). As shown in Fig. 3d, despite some Cu^+ ions having been oxidized into Cu^{2+}, the XRD patterns indicate that the products still remain in the pure cubic Cu_2O phase [29].

The morphology evolution of Cu_2O with CS and NCS as supports is revealed by TEM images (Fig. 2e and f). It was found that Cu_2O nanoparticles are better dispersed on NCS compared to CS. As Han et al. [30] reported, the nitrogen-doped carbon skeleton with abundant defects can increase the stability as well as inhibit the aggregation of Cu_2O nanoparticles. As depicted in Table S1, the nitrogen content in CS is calculated to be 1.90 at%, which is derived from petroleum pitch [31]. While in the NCS, the nitrogen content was raised to 3.18 at% due to the post nitrogen doping using urea as nitrogen source, indicating the high nitrogen content plays a key role in controlling the dispersion of Cu_2O nanocrystals on carbon materials. It is interesting that the morphology of Cu_2O on the CS is near spherical while the Cu_2O on the NCS is cubic. This special phenomenon may be attributed to the fine structure of the defects and functional groups on the surface of CS and NCS, which needs further investigation.

The catalytic performance of CS and NCS are shown in Fig. S5. Under all measured potentials, H_2 is the main product and CO_2 can only be reduced to CO and HCOOH on the two carbon materials. Compared with CS, NCS has a higher selectivity of CO at the same potential, indicating nitrogen doping can facilitate the CO_2 electroreduction on carbon material. None hydrocarbons were found in the gas and liquid products on CS and NCS catalysts, indicating Cu_2O is the main active site in the composites for ethylene formation during CO_2 electroreduction.

The catalytic performance of Cu_2O, Cu_2O/CS and Cu_2O/NCS was investigated and the results are shown in Fig. 4. Along with the increasing potential, the FE of C_2H_4 arises gradually and achieves the highest value at −1.3 V *vs.* RHE. With further increasing the potential, the FE of C_2H_4 declines mainly due to the competitive CH_4 formation [32]. Among the three catalysts, Cu_2O/NCS behaves the highest FE of C_2H_4 (24.7%) with remarkable durability, which is attributed to the well dispersion of Cu_2O nanoparticles and the abundant pyridinic-N in NCS. The pyridinic-N structure has been reported as a CO_2 and proton absorber, facilitating hydrogenation and C−C coupling reactions on Cu-based materials for the formation of C_2H_4 [33]. As shown in Figs. S6a and S6b, HER is significantly inhibited and more CO is produced on the composites compared with pristine Cu_2O, indicating the catalytic activity of Cu_2O towards CO_2 electroreduction is effectively improved by supporting on the carbon materials as made, especially for NCS. Carbon monoxide has been proposed to be an important intermediate, which is further reduced to CH_4 and C_2H_4 on copper-based catalysts during CO_2 electroreduction [34]. Furthermore, we found the CH_4 was totally suppressed on Cu_2O/NCS (Fig. S6c) compared to Cu_2O/CS, indicating the nitrogen moieties in carbon material play a key role in promoting C_2H_4 formation rather than CH_4 on Cu_2O. For liquid products (Fig. S6d), the selectivity of HCOOH was remarkably higher on Cu_2O/CS compared with Cu_2O/NCS, especially under lower potentials. This phenomenon may be attributed to the spherical morphology and serious aggregation of Cu_2O on CS.

To further study the catalytic stability of Cu_2O, Cu_2O/CS and Cu_2O/NCS catalysts, the long-term electrocatalysis of CO_2 tests are

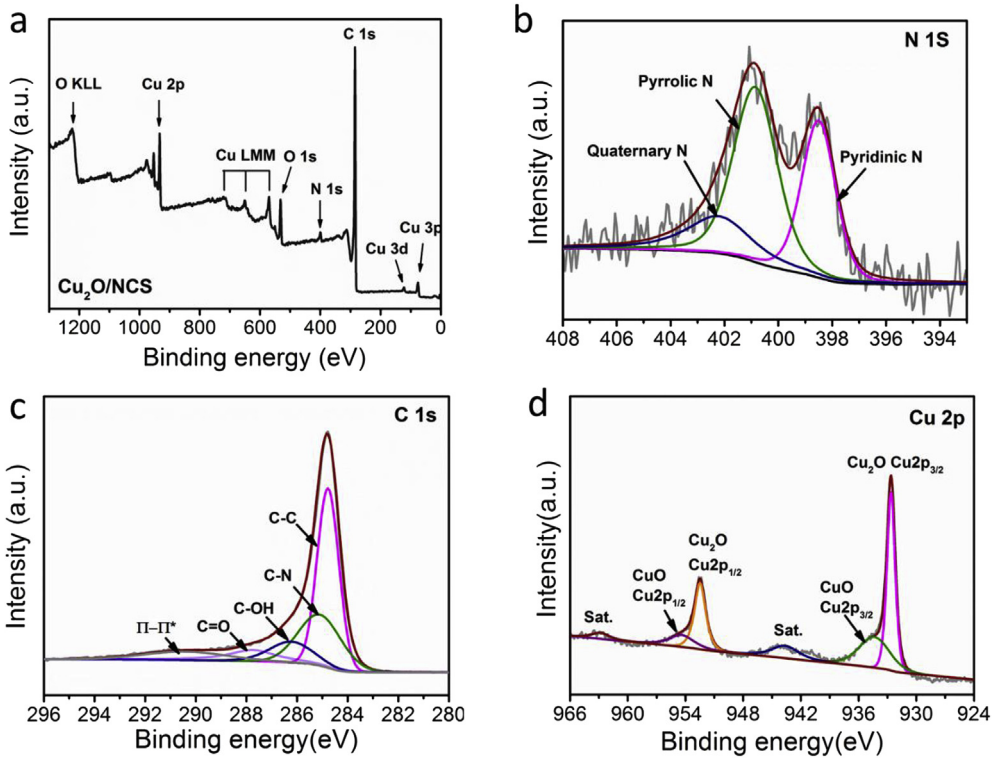

Fig. 3. (a) XPS survey spectra of Cu_2O/NCS catalyst. High-resolution XPS signals of Cu_2O/NCS (b) N 1s, (c) C 1s and (d) Cu 2p. (A colour version of this figure can be viewed online.)

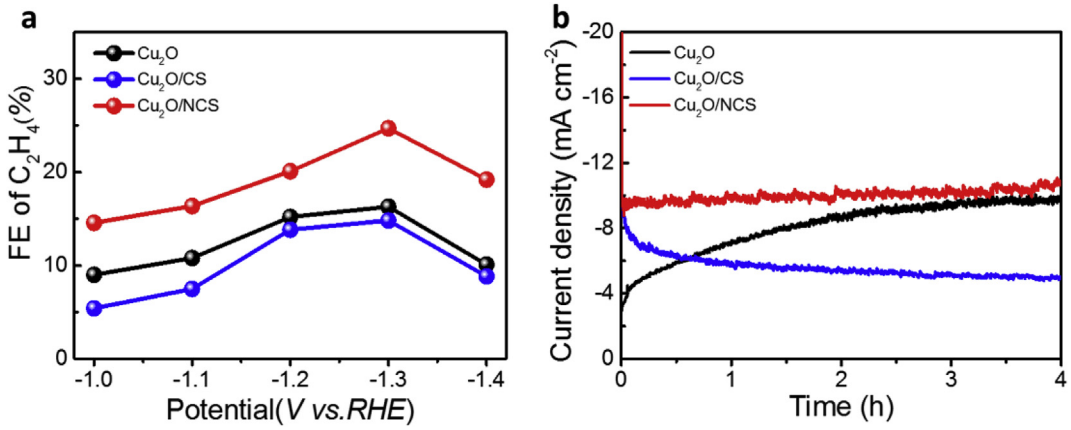

Fig. 4. (a) Faradaic efficiencies of C_2H_4 on Cu_2O, Cu_2O/CS and Cu_2O/NCS catalysts at different potentials; (b) Long-term performance at −1.3 V *vs.* RHE. (A colour version of this figure can be viewed online.)

carried out at −1.3 V for 4 h. As depicted in Fig. 4b, the current density of pure Cu_2O catalysts increases as the reaction proceeds due to the reduction of Cu_2O to Cu under negative potential [7]. In contrast, the current density of Cu_2O/CS decreases due to the leaching of aggregated Cu_2O during CO_2 electroreduction. As shown in Fig. 4b, Cu_2O/NCS presents the highly stable current density, which may be explained by local pH effect. Due to the hydrogen evolution reaction catalyzed by CS and NCS, OH^- is generated on the surface of catalysts. Because of the confinement effect of CS and NCS, the neutralization reaction of OH^- with bicarbonate in the electrolyte is hampered, resulting in higher local pH near the Cu_2O nanocrystals compared to bulk solutions. Mistry et al. [19] reported the high pH facilitates the stabilization of Cu^+ on the surface of Cu_2O against the reduction potential by negatively shifting the reduction over potential of Cu^+ to Cu^0. Therefore, the high local pH will facilitate the durability of Cu_2O as catalyst for CO_2 electroreduction. Based on above concepts, both the microstructure and the high pyridinic-N moieties of the carbon materials are critical to the excellent electrochemical stability of Cu_2O during the CO_2 reduction.

4. Conclusions

In summary, we proposed a facile strategy to uniformly disperse the cubic Cu_2O nanocrystals on a nitrogen doped petroleum asphalt-based carbon material. The obtained Cu_2O/NCS composites have a high FE of C_2H_4 (24.7%) and remarkable stability for at least 4 h as catalyst for CO_2 electroreduction at −1.3 V (*vs.* RHE). The excellent performance of Cu_2O/NCS is attributed to the following aspects: (1) The ultra-thin shell structure and high N doping content of NCS facilitate the uniform dispersion of Cu_2O nanocubes, which is benefit for the effective exposure of Cu active sites. (2) The abundant pyridinic-N species in NCS promote the adsorption and protonation of CO_2 on the catalyst surface, further enhance the catalytic selectivity of Cu_2O towards C_2H_4. Further studies are needed to characterize the composition and morphology of Cu_2O catalysts in operando and to reveal the detailed synergetic mechanism of Cu_2O and pyridinic-N for boosting C_2H_4 selectivity by NCS supports.

Acknowledgements

This work is financially supported by the National Natural Science Foundation of China (Nos. 51572296, U1662113, 51372277); the Shandong Provincial Natural Science Foundation (ZR2018BB070); the CAS Key Laboratory of Carbon Materials (KLCMKFJJ1706); the Fundamental Research Funds for the Central Universities of China (18CX02015A), the Financial Support from Taishan Scholar Project of Shandong Province of China.

Appendix A. Supplementary data

Supplementary data to this article can be found online at https://doi.org/10.1016/j.carbon.2019.02.010.

References

[1] C.C. Yan, H.B. Li, Y.F. Ye, H.H. Wu, F. Cai, R. Si, et al., Coordinatively unsaturated nickel-nitrogen sites towards selective and high-rate CO_2 electroreduction, Energy Environ. Sci. 11 (2018) 1204–1210.
[2] M.W. Jia, Q. Fan, S.Z. Liu, J.S. Qiu, Z.Y. Sun, Single-atom catalysis for electrochemical CO_2 reduction, Current Opinion in Green and Sustainable Chemistry 16 (2019) 1–6.
[3] L. Zhang, Z.J. Zhao, T. Wang, J.L. Gong, Nano-designed semiconductors for electro- and photoelectro-catalytic conversion of carbon dioxide, Chem. Soc. Rev. 47 (2018) 5423–5443.
[4] W.Y. Deng, L. Zhang, H. Dong, X.X. Chang, T. Wang, J.L. Gong, Achieving convenient CO_2 electroreduction and photovoltage in tandem using potential-insensitive disordered Ag nanoparticles, Chem. Sci. 9 (2018) 6599–6604.
[5] W.J. Zhu, L. Zhang, P.P. Yang, C.L. Hu, Z.B. Luo, X.X. Chang, Z.J. Zhao, J.L. Gong, Low-coordinated edge sites on ultrathin palladium nanosheets boost carbon dioxide electroreduction performance, Angew. Chem. Int. Ed. 57 (2018) 11544–11548.
[6] L. Zhang, Z.J. Zhao, J.L. Gong, Nanostructured materials for heterogeneous electrocatalytic CO_2 reduction and their related reaction mechanisms, Angew. Chem. Int. Ed. 56 (2017) 11326–11353.
[7] D. Ren, Y. Deng, A.D. Handoko, C.S. Chen, S. Malkhandi, B.S. Yeo, Selective electrochemical reduction of carbon dioxide to ethylene and ethanol on copper(I) oxide catalysts, ACS Catal. 5 (2015) 2814–2821.
[8] R.A. Geioushy, M.M. Khaled, A.S. Hakeem, K. Alhooshani, C. Basheer, High efficiency graphene/Cu_2O electrode for the electrochemical reduction of carbon dioxide to ethanol, J. Electroanal. Chem. 785 (2017) 138–143.
[9] D. Kim, S. Lee, J.D. Ocon, B. Jeong, J.K. Lee, J. Lee, Insights into an autonomously formed oxygen-evacuated Cu_2O electrode for the selective production of C_2H_4 from CO_2, Phys. Chem. Chem. Phys. 17 (2015) 824–830.
[10] Q.C. Wang, Y.P. Lei, Z.Y. Chen, N. Wu, Y.B. Wang, B. Wang, et al., Fe/Fe_3C@C nanoparticles encapsulated in N-doped graphene–CNTs framework as an efficient bifunctional oxygen electrocatalyst for robust rechargeable Zn–air batteries, J. Mater. Chem. A 6 (2018) 516–526.
[11] K.L. Lv, Y.C. Fan, Y. Zhu, Y. Yuan, J.R. Wang, Y. Zhu, et al., Elastic Ag-anchored N-doped graphene/carbon foam for the selective electrochemical reduction of carbon dioxide to ethanol, J. Mater. Chem. A 6 (2018) 5025–5031.
[12] R.A. Geioushy, M.M. Khaled, K. Alhooshani, A.S. Hakeem, A. Rinaldi, Graphene/ZnO/Cu_2O electrocatalyst for selective conversion of CO_2 into n-propanol, Electrochim. Acta 245 (2017) 456–462.
[13] J. Gu, F. Heroguel, J. Luterbacher, X. Hu, Densely packed, densely packed, ultra small SnO nanoparticles for enhanced activity and selectivity in electrochemical CO_2 reduction, Angew. Chem. Int. Ed. 57 (2018) 2943–2947.
[14] M.W. Jia, C. Choi, T.S. Wu, C. Ma, P. Kang, H.C. Tao, et al., Carbon-supported Ni nanoparticles for efficient CO_2 electroreduction, Chem. Sci. 9 (2018)

8767–8896.
[15] C.H. Zhang, S.Z. Yang, J.J. Wu, M.J. Liu, S. Yazdi, M.Q. Ren, et al., Electrochemical CO_2 reduction with atomic iron-dispersed on nitrogen-doped graphene, Adv. Energy Mater. 8 (2018) 1703487.
[16] H.Q. Li, N. Xiao, M.Y. Hao, X.D. Song, Y.W. Wang, Y.Q. Ji, et al., Efficient CO_2 electroreduction over pyridinic-N active sites highly exposed on wrinkled porous carbon nanosheets, Chem. Eng. J. 351 (2018) 613–621.
[17] K. Saravanan, E. Gottlieb, J.A. Keith, Nitrogen-doped nanocarbon materials under electroreduction operating conditions and implications for electrocatalysis of CO_2, Carbon 111 (2017) 859–866.
[18] Q. Li, W.L. Zhu, J.J. Fu, H.Y. Zhang, G. Wu, S.H. Sun, Controlled assembly of Cu nanoparticles on pyridinic-N rich graphene for electrochemical reduction of CO_2 to ethylene, Nanomater. Energy 24 (2016) 1–9.
[19] H. Mistry, A.S. Varela, C.S. Bonifacio, I. Zegkinoglou, I. Sinev, Y.W. Choi, et al., Highly selective plasma-activated copper catalysts for carbon dioxide reduction to ethylene, Nat. Commun. 7 (2016) 12123.
[20] J.Y. Liu, Y. Liu, P. Li, L.H. Wang, H.R. Zhang, H. Liu, et al., Fe-N-doped porous carbon from petroleum asphalt for highly efficient oxygen reduction reaction, Carbon 126 (2018) 1–8.
[21] Y.X. Wang, Y.W. Wang, J.L. Liu, L. Pan, W. Tian, M.B. Wu, et al., Preparation of carbon nanosheets from petroleum asphalt via recyclable molten-salt method for superior lithium and sodium storage, Carbon 122 (2017) 344–351.
[22] Z.T. Li, R.F. Xu, S.Z. Deng, X. Su, W.T. Wu, S.P. Liu, et al., MnS decorated N/S codoped 3D graphene which used as cathode of the lithium-sulfur battery, Appl. Surf. Sci. 433 (2018) 10–15.
[23] P. Li, J.Y. Liu, Y. Liu, Y.W. Wang, Z.T. Li, W.T. Wu, et al., Three-dimensional $ZnMn_2O_4$/porous carbon framework from petroleum asphalt for high performance lithium-ion battery, Electrochim. Acta 180 (2015) 164–172.
[24] Z. Weng, Y.S. Wu, M.Y. Wang, J.B. Jiang, K. Yang, S.J. Huo, et al., Active sites of copper-complex catalytic materials for electrochemical carbon dioxide reduction, Nat. Commun. 9 (2018) 415.
[25] X.F. Bai, W. Chen, C.C. Zhao, S.G. Li, Y.F. Song, R.P. Ge, et al., Exclusive formation of formic acid from CO_2 electroreduction by a tunable Pd-Sn alloy, Angew. Chem. Int. Ed. 56 (2017) 12219–12223.
[26] Y. Mao, H. Duan, B. Xu, L. Zhang, Y.S. Hu, C.C. Zhao, et al., Lithium storage in nitrogen-rich mesoporous carbon materials, Energy Environ. Sci. 5 (2012) 7950–7955.
[27] Y. Wang, D.C. Alsmeyer, R.L. McCreery, Raman spectroscopy of carbon materials: structural basis of observed spectra, Chem. Mater. 2 (1990) 557–563.
[28] J.J. Wu, R.M. Yadav, M.J. Liu, P.P. Sharma, C.S. Tiwary, L.L. Ma, et al., Achieving highly efficient, selective, and stable CO_2 reduction on nitrogen-doped carbon nanotubes, ACS Nano 9 (2015) 5364–5371.
[29] Y. Zhang, X. Wang, L. Zeng, S.Y. Song, D.P. Liu, Green and controlled synthesis of Cu_2O-graphene hierarchical nanohybrids as high-performance anode materials for lithium-ion batteries via an ultrasound assisted approach, Dalton Trans. 41 (2012) 4316–4319.
[30] X.G. Han, X.X. He, L.M. Sun, X. Han, W.W. Zhan, J.H. Xu, et al., Increasing effectiveness of photogenerated carriers by in situ anchoring of Cu_2O nanoparticles on a nitrogen-doped porous carbon yolk–shell cuboctahedral framework, ACS Catal. 8 (2018) 3348–3356.
[31] P. Li, J.Y. Liu, Y.W. Wang, Y. Liu, X.N. Wang, K.W. Nam, et al., Synthesis of ultrathin hollow carbon shell from petroleum asphalt for high-performance anode material in lithium-ion batteries, Chem. Eng. J. 286 (2016) 632–639.
[32] S.Y. Lee, H. Jung, N.K. Kim, H.S. Oh, B.K. Min, Y.J. Hwang, Mixed copper states in anodized Cu electrocatalyst for stable and selective ethylene production from CO2 reduction, J. Am. Chem. Soc. 140 (2018) 8681–8689.
[33] Y.W. Lum, Y.K. Kwon, P. Lobaccaro, L. Chen, E.L. Clark, A.T. Bell, et al., Trace levels of copper in carbon materials show significant electrochemical CO_2 reduction activity, ACS Catal. 6 (2016) 202–209.
[34] Y. Huang, A.D. Handoko, P. Hirunsit, B.S. Yeo, Electrochemical reduction of CO_2 using copper single-crystal surfaces: effects of CO^* coverage on the selective formation of ethylene, ACS Catal. 7 (2017) 1749–1756.